Ceramide-based nanostructured lipid carriers for transdermal delivery of isoliquiritigenin: Development, physicochemical characterization, and *in vitro* skin permeation studies

Geun Young Noh, Ji Young Suh, and Soo Nam Park[†]

Cosmetic R&D Center, Department of Fine Chemistry, Cosmetic Industry Coupled Collaboration Center,
Seoul National University of Science and Technology, 232 Gongneung-ro, Nowon-gu, Seoul 01811, Korea
(*Received 20 May 2016 • accepted 23 September 2016*)

Abstract−An optimized, ceramide-based, nanostructured lipid carrier (NLC) formulation was developed for isoliquiritigenin (ILTG), and its potential as a transdermal delivery system was evaluated. ILTG-loaded NLCs were prepared by blending solid (ceramide, cholesterol) and liquid lipids (caprylic/capric triglyceride) in various proportions using a hot homogenization and ultrasonication method. The physicochemical characteristics were investigated by DLS, ZP, EE%, TEM, DSC and XRD analyses and *in vitro* skin permeation studies. The results showed that the particle size of the formulation was 150.19-251.69 nm with a ZP>−20 mV. The EE% was 56.45-89.97%. The NLC structure was influenced by lipid ratio, and increasing the caprylic/capric triglyceride ratio caused a less ordered structure, as confirmed by DSC. The XRD analysis indicated that ILTG was not in the crystalline state in all formulations. The skin permeation study showed that the ILTG-NLCs promoted ILTG permeation. In conclusion, ceramide-based NLCs could be a promising vehicle for the ILTG transdermal delivery of ILTG.

Keywords: Nanostructured Lipid Carrier, Transdermal Delivery System, Ceramide, Isoliquiritigenin, MEL

INTRODUCTION

The barrier function of the stratum corneum is attributed to the multi-lamellar structure of keratin cells and the intercellular lipids between them. Intercellular lipids are composed of ceramides, cholesterols, and free fatty acids. They protect the skin from physical stimulation and induce skin homeostasis [1,2]. Ceramides are the major lipids of the stratum corneum and play an important role in the skin. A decreased quantity of ceramides in the skin leads to a reduction in skin barrier function. Several studies have cited this as the primary cause of atopic dermatitis, psoriasis, and ichthyosis [3-5]. Ceramides contain a polar amide group, nonpolar long alkyl chains, and two to three hydroxyl groups that lead to weak polarity. The hydroxyl groups and amide groups of ceramides form a lamellar structure through a hydrogen bonding with the carboxyl groups of fatty acids present in the intercellular lipids [6]. The skin is the most common route of transdermal drug delivery. Using a transdermal delivery system with intercellular lipid ingredients can ensure effective delivery of drugs through the intercellular pathway [7-9].

Lipid nanoparticles are an effective delivery system for poorly soluble drugs such as isoliquiritigenin (ILTG) and offer several advantages, such as resolution of problems related to the high cost of manufacturing, ease of large-scale production and improvement of physical stability in comparison to that of liposomes, microparticles, and oil-in-water (o/w) emulsions [10]. In addition, lipid nanopar-

ticles are highly adhesive to the skin surface because they form a thin lipid film on it. The lipid film prevents evaporation of water from skin, and promotes absorption by enabling the continuous release of active material through the carriers [11].

The so-called first-generation lipid nanoparticles, solid lipid nanoparticles (SLNs), and the improved second-generation SLNs, namely, the nanostructured lipid carriers (NLCs) [12], are two delivery systems that exist as partly solid matrices at room temperature or body temperature and have crystalline characteristics. Liquid lipid NLCs have the following manufacturing conditions: imperfect type, amorphous, and multiples types [13]. In particular, NLCs have different chemical properties depending on the composition and proportion of the lipids used. Therefore, when producing NLCs loaded with a particular drug, it is important to evaluate the physicochemical characteristics to select an optimum transdermal delivery system [14].

ILTG (2′,-4′,-4-trihydroxychalcone) is a compound isolated from *Glycyrrhiza uralensis*, which has various pharmacological activities such as antioxidant, anti-inflammatory, anticancer, anti microbial, skin-whitening, and cellular protective effects [15-18]. The
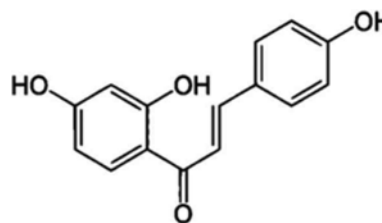

Fig. 1. Chemical structure of isoliquiritigenin (ILTG).

[†]To whom correspondence should be addressed.
E-mail: snpark@seoultech.ac.kr

molecular structure of ILTG is shown in Fig. 1. ILTG, however, has drawbacks in product application owing to its low solubility [19]. To overcome this disadvantage, ILTG has been incorporated into transdermal delivery systems, which enhances the skin permeation of the active ingredients. In our previous study, we performed various experiments using transdermal delivery systems and functional materials with antioxidant, antiaging, and antibacterial properties to examine their ability to deliver drugs effectively [20-24]. We developed ceramide-based, ILTG-loaded, nanostructured lipid carriers (ILTG-NLCs). Furthermore, we investigated their physicochemical properties and conducted an *in vitro* skin permeation study based on the ratios of solid and liquid lipids. These studies were performed to confirm whether the ILTG-NLCs were suitable carriers for the transdermal delivery of ILTG.

MATERIALS AND METHODS

1. Materials

The solid lipid ceramide (DS-CERAMIDE Y30) was kindly provided by Doosan Co., (Seoul, Korea), cholesterol (purity ≥99.0%) was purchased from Sigma-Aldrich (St. Louis, MO, U.S.A.). The liquid lipid caprylic-capric triglyceride was provided by Saimdang Co., Ltd., (Cheongju, Korea). Surfactants for the lipid carriers Tween® 80 were donated by Saimdang Co., Ltd. (Cheongju, Korea) and mannosylerythritol lipid (MEL) was obtained from Toyobo Co., (Japan). The other solvents used such as ethanol (EtOH) and acetone were of analytical grade. ILTG (purity ≥97.0%) and D-(+)-glucose (purity ≥98.0) were purchased from Sejin Co., (Seoul, Korea).

2. Development of ILTG-NLCs

All lipid carriers were prepared using a homogenization and ultrasonication method, and the composition ratios of ILTG-NLC and ILTG-nanoemulsion (NE) are shown in Table 1. Briefly, a solid lipid phase (ceramide : cholesterol, 8 : 2 w/w%) mixture, caprylic-capric triglyceride, and MEL were dissolved on a water bath at 80 °C, and stirred at 300 rpm for 20 min. Then, the ILTG solution (dissolved in acetone : EtOH, 1 : 1 v/v%) was poured into the solid lipid phase, and the mixture was stirred at 500 rpm for 3 min. At the same time, the aqueous phase was prepared by dissolving Tween® 80 in purified water and heating at 70 °C. After melting the lipid phase, the aqueous phase was added, and the mixture was homogenized using a homogenizer (Ultra Turrax®T25 Basic, IKA® Korea. Ltd., Seoul, Korea) at 14,000 rpm for 2 min. The hot pre-emulsion obtained was ultrasonicated with 50% amplitude for 10 min using an ultrasonicator (Branson Korea Co., Ltd., Gunpo, Korea). During the homogenization and ultrasonication processes, a constant temperature of 70 °C was maintained. The O/W nanoemulsion (NE)

formed was immediately cooled to 4 °C at 500 rpm for 15 min. Finally, the ILTG-NLC suspension was prepared, and the ILTG-NE was not cooled.

3. Physicochemical Characterization

3-1. Particle Size and Zeta Potential Analysis

The mean particle size (z-ave), polydispersity index (PDI) and zeta potential (ZP) were determined using dynamic light scattering (DLS) with a particle size and zeta potential analyzer (Els-Z series, Otsuka Electronics Korea, Seongnam, Korea). The ILTG-NLCs and ILTG-NE were diluted with double distilled water to a suitable scattering intensity and analyzed at 25 °C with a 165° scattering angle. All measurements were performed in triplicate.

3-2. Entrapment Efficiency (EE%)

The prepared ILTG-NLCs and ILTG-NE suspensions were filtered through a 5-μm syringe filter (Minisart CA, USA, 26-mm) to remove any free ILTG crystals. Then, methanol was added to the filtered ILTG-NLC and ILTG-NE dispersions and sonicated for 1 h to extract ILTG from the lipid. Methanol was evaporated using a rotary evaporator, and the residue was re-dissolved in 1 mL methanol. The amount of ILTG incorporated was detected with an ultraviolet-visible (UV-Vis) spectrophotometer (Varian, Australia, Cary50) at a detection wavelength of 372 nm. In addition, the entrapment efficiency (EE%) of ILTG was calculated using Eq. (1).

$$EE\% = W_{entrapped}/W_{initial} \times 100 \tag{1}$$

where, $W_{entrapped}$ is the amount of ILTG passing through 5-μm syringe filter, and $W_{initial}$ is the initially added amount of ILTG.

3-3. Transmission Electron Microscope (TEM) Examination

The morphology of ILTG-NLCs and ILTG-NE dispersion were observed using transmission electron microscopy (TEM) using a JEOL-JEM1010 instrument (JEOL Ltd., Tokyo, Japan). The samples were diluted five-fold with double distilled water on a 200-mesh copper grid and negatively stained with 0.2% (w/v%) phosphotungstic acid and dried for 30 s. The analysis was performed at an accelerating voltage of 80 kV.

3-4. Differential Scanning Calorimetry (DSC) Analysis

The differential scanning calorimetry (DSC) analysis was performed using a Shimadzu DSC-60 series instrument (Dong-il Shimadzu Corp., Seoul, Korea). The samples were accurately weighed (1.5 mg) based on the lipid content of the NLC and NE dispersions were placed in 40-μL aluminum pans. The samples were analyzed at a heating rate of 5 °C/min from 25 to 100 °C. During the measurements, the pans were purged using nitrogen gas (50 mL/min) and empty aluminum pans were used as the reference. The data were analyzed using the Ta-60 software. Additionally, the crystallinity indices (CI %) of ILTG-NLCs were calculated using Eq. (2).

Table 1. Compositions of isoliquiritigenin-loaded nanostructured lipid carrier (ILTG-NLC) and ILTG-nanoemulsion (NE) formulations

Formulation	Total lipid 5 (% w/v)		ILTG (%)	Surfactant 2 (% w/v)	
	Solid lipid (%)	Liquid lipid (%)		Tween 80	MEL
ILTG-NLC1	70	30	0.05	1.5	0.5
ILTG-NLC2	50	50	0.05	1.5	0.5
ILTG-NLC3	30	70	0.05	1.5	0.5
ILTG-NE	-	100	0.05	1.5	0.5

$$CI(\%) = \frac{\Delta H_{ILTG\text{-}NLC\ aqueous\ dispersion}}{\Delta H_{lipid\ bulk} \times Concentration_{lipid\ phase}} \times 100\% \qquad (2)$$

where, $\Delta H_{ILTG\text{-}NLC\ aqueous\ dispersion}$ and $\Delta H_{lipid\ bulk}$ are melting enthalpy (J/g) of the ILTG-NLC dispersion and lipid bulk, respectively.

3-5. X-ray Diffraction Analysis

The X-ray diffraction (XRD) analysis involved a powder X-ray diffractometer with a D8 advance (Bruker, Germany). It was performed with a copper anode (Cu-kα radiation, 40 kV, 40 mA, $\lambda=$ Cu kα1 - 1.5418 Å), using an LYNXEYE XE as a detector. The samples were scanned over a 2 Theta range of 3-50 degree. The measured samples were pure ILTG, solid lipid (ceramide and cholesterol mixture), a physical mixture, freeze-dried ILTG-NLC, and ILTG-NE.

4. *In Vitro* Skin Permeation Study

An *in vitro* skin permeation study was performed to investigate the enhancing effects of ILTG-NLCs and ILTG-NE on the skin permeation of ILTG using the Franz diffusion cell. Dorsal skin samples of ICR mice (7-week-old) were used in the skin permeation study. The receptor chamber was filled with phase (5 mL HCO-60 : EtOH : phosphate-buffered saline (PBS), 2 : 20 : 78 w/w/w%) and stirred at 150 rpm for 24 h. The skin was fixed between the donor and the receptor phase, with the stratum corneum side facing the donor compartment. Samples (0.2 mL) were applied to the skin in the donor compartment. The skin area contacting the receptor phase was 0.6362 cm^2, and the receptor medium was kept at 37 $^\circ$C throughout the experiment using a constant temperature water bath. At fixed time intervals (3, 6, 9, 12, and 24 h), 0.5 mL of the receptor phase was collected and replaced with fresh receptor phase. The amount of ILTG in the sample was analyzed using a UV spectrophotometer (Varian, Australia, Cary50). The amount of ILTG retained in the skin was determined at the end of the *in vitro* permeation experiment (24 h). The skin surface was washed with PBS solution on each side to remove the residual donor samples. The stratum corneum was removed using the tape-stripping method thrice with 3M scotch tape (Korea 3M), and the skin was dissolved in 100% EtOH using a sonicator for 1 h. The concentrations of extracted ILTG were determined using the UV spectrophotometer.

RESULTS AND DISCUSSION

1. Physicochemical Properties of ILTG-NLC and ILTG-NE

1-1. Particle Size, PDI, and Zeta Potential (ZP)

Lipid carriers can be prepared using various composition ratios of solid and liquid lipids. In this study, 0.05% ILTG-loaded NLC and NE were used with lipid forming 5% of the total formulation. The composition ratio of solid and liquid lipid in NLC1, NLC2, and NLC3 was 70 : 30, 50 : 50, and 30 : 70, respectively, while the NE was composed of 100% liquid lipid. The mean particle size of ILTG-NLCs and ILTG-NE is shown in Fig. 2(a). The average particle diameters of the ILTG-NLC1, ILTG-NLC2, ILTG-NLC3, and ILTG-NE were 251.6±6.89 nm, 208.7±2.95 nm, 152.2±2.12 nm, and 151.9±1.59 nm respectively. Increasing the amount of the liquid lipid to 30 (NLC1), 50 (NLC2), 70 (NLC3), and 100% (NE) lowered the viscosity of NLC and NE and resulted in smaller par-
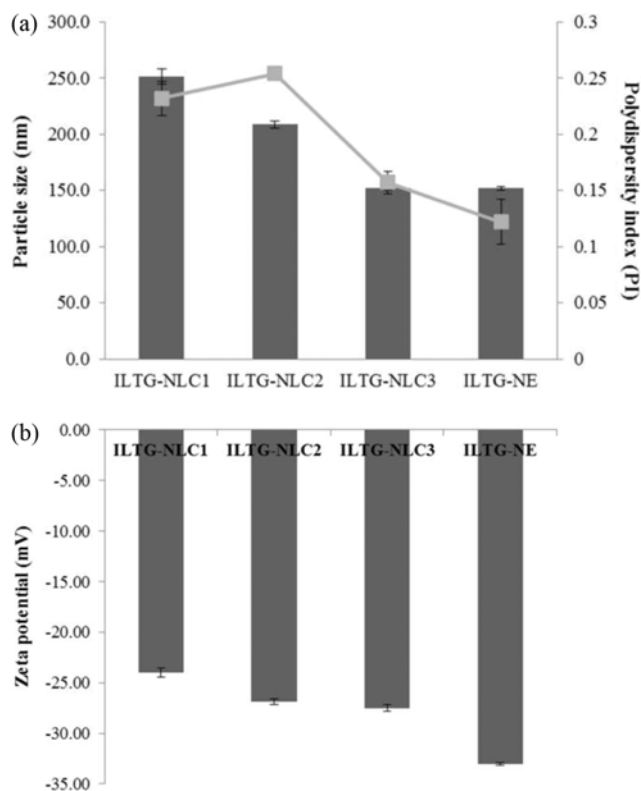

Fig. 2. (a) Average particle size, polydispersity index (PDI), and (b) zeta potential (ZP) of isoliquiritigenin-loaded nanostructured lipid carrier (ILTG-NLCs) and ILTG-nanoemulsion (NE).

ticle sizes. According to previous studies, the mean particle size of lipid nanoparticles generally depends on lipid type, the concentration of surfactant, and the viscosity of the lipid phase [25]. In this study, the concentration of the surfactant was the same and, therefore, the viscosity of the total lipid phase had a major influence on the particle size. ILTG-NE comprising the liquid lipid and ILTG-NLC3 comprising 30% solid lipid had approximately the same particle size. When the liquid lipid content was >70%, the viscosity was similar [26,27]. The PDI indicates the homogeneity of particles. and the measured values were <0.3.

ZP is the electric charge on the particle surface that confers emulsion stability at appropriate values. The ZP values of all the developed formulations are shown in Fig. 2(b). As shown, ZP values of ILTG-NLC1, ILTG-NLC2, ILTG-NLC3, and ILTG-NE were −24.01± 0.44 mV, −26.85±0.27 mV, −27.49±0.37 mV, ILTG-NE and, −33.02± 0.11 mV, respectively. The stability of the developed formulations supports the maintenance of a favorable ZP value above −20 mV. Increasing the content of caprylic/capric triglyceride (liquid lipid) increased the ZP value. This is attributable to the increase in the number of carboxylic groups in the caprylic/capric triglyceride. Therefore, the ZP values were the highest for the NE consisting of 100% liquid lipid. Furthermore, we expected steric stability from the non-ionic surfactants Tween 80 and MEL [28,29].

1-2. Entrapment Efficiency (EE%)

The EE% is defined as the percentage of drug incorporated into the carriers in comparison to the total drug added. It is an important parameter in evaluating the loading capacity of developed for-
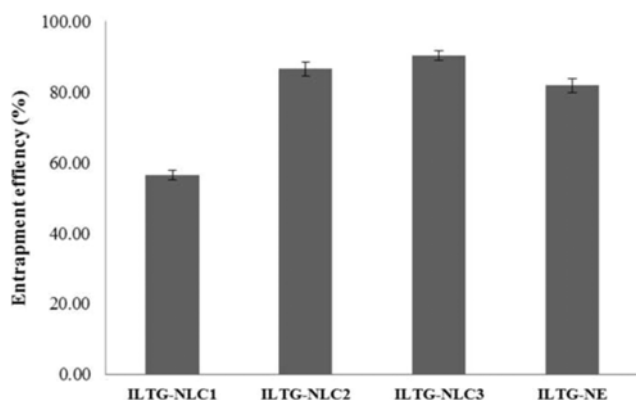
Fig. 3. Entrapment efficiency (EE%) of isoliquiritigenin-loaded nanostructured lipid carrier (ILTG-NLCs) and ILTG-nanoemulsion (NE).

Fig. 5. Differential scanning calorimetry (DSC) thermograms (a) solid lipid bulk, (b) isoliquiritigenin-loaded nanostructured lipid carrier (ILG-NLC) 1, (c) ILTG-NLC2, (d) ILTG-NLC3, and (e) ILTG-nanoemulsion (NE).

mulations [30]. The results obtained are shown in Fig. 3. ILTG-NLC3 showed the highest entrapment of 89.97±1.71%. The EE% of ILTG-NLC2, ILTG-NE, and ILTG-NLC1 was 86.50±1.89%, 81.86±1.97%, and 56.45±1.31%, respectively. The lowest EE% was observed for ILTG-NLC1. This result might be because the solubility of ILTG in liquid lipid is greater than that in solid lipid. In addition, it could have been due to the increase in ceramide content, which led to the formation of a more rigid lipid particles and reduced the space available to incorporate the drug [31]. The EE%

of the NE was 81.86%, which was slightly lower than that of NLC2 and NLC3. Therefore, both the liquid lipid and solid lipid were found to affect the EE%. Ceramide has long hydrocarbon chains, which can affect the solubility of ILTG [32]. From these results, the lipid blending ratio should be considered in strategies to improve the EE%.

1-3. TEM Analysis

The morphology of the ILTG-loaded lipid carriers was determined using TEM Fig. 4. The particles were spherical, approximately 200 nm, and had no rod-like particles. The average particle size obtained using TEM was similar to the results of the DLS analysis. The low PDI indicated a uniform particle dispersion image.

1-4. DSC Analysis

The DSC measurements confirmed the crystallization and thermal behavior of the lipid nanoparticles [33]. The main purpose of this study was to investigate lipid particles and compare their crystallinity and thermal behavior with that of the raw material used in the preparation. The bulk lipid was measured by mixing the ceramide and cholesterol at a ratio of 8 : 2. The melting points of the developed formulations were compared with those of the main lipid ceramide, which showed a distinct peak (Fig. 5). From these results, the melting point, onset temperatures, and enthalpy depression occurred when the NLC was formed. The melting points of ILTG-NLC1, ILTG-NLC2, ILTG-NLC and the bulk lipid were 89.87 °C, 76.94 °C, 76.82 °C, and 93.41 °C, respectively. The melting point depression phenomena occurred because of the small particles, which were in the nanometer size range and had a high specific sur-
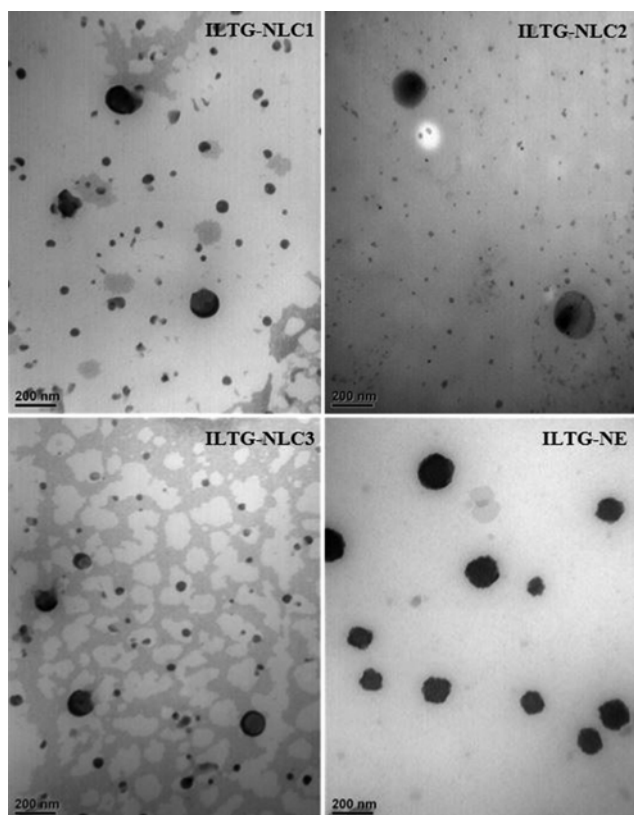

Fig. 4. Transmission electron microscopy (TEM) images of isoliquiritigenin-loaded nanostructured lipid carrier (ILTG-NLCs) and ILTG-nanoemulsion (NE).
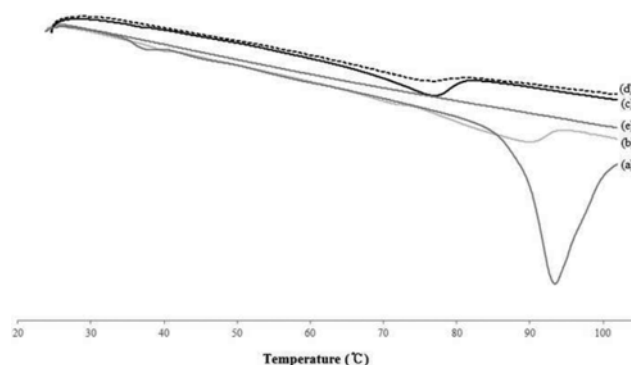
Table 2. Differential scanning calorimetry (DSC) parameters of bulk lipid and isoliquiritigenin-loaded nanostructured lipid carriers (ILTG-NLCs) and ILTG-nanoemulsion (NE)

Formulation	On set (°C)	Melting point (°C)	Enthalpy (J/g)	CI (%)
ILTG-NLC1	76.05	89.87	18.34	50.50
ILTG-NLC2	71.81	76.94	9.76	26.88
ILTG-NLC3	68.09	76.82	5.06	13.93
ILTG-NE	0	0	0	0
Solid lipid bulk	35.36	38.27	1.28	100
	89.48	93.41	71.35	

face area [34]. Table 2 shows the DSC parameters of all the developed ILTG-NLCs. Fig. 5 shows the DSC thermograms, and those of the ILTG-NE did not show any phase change, because there was no solid lipid present. As the liquid lipid content increases, and that of the solid lipid including the ceramide decreases, broad peaks are expected. Furthermore, as the crystallinity decreased, a broader peak was observed. The findings of the crystallinity analysis showed that ILTG-NLC1, ILTG-NL2, and ILTG-NLC3 were 50.05%, 26.88%, and 13.93% crystalline, respectively. Thus, NLC may exist in a similar form as that of the particles of an O/W emulsion [35]. Additionally, a lower crystallinity is indicative of a rigid formulation. This factor can be considered as a strategy for increasing the space to enhance the ILTG EE%.

1-5. XRD Analysis

To identify the physical state of the ILTG incorporated in the NLCs and NE XRD was used. X-ray diffractograms of solid lipid (ceramide : cholesterol, 8 : 2), pure ILTG, and drug-lipid physical mixture as well as the lyophilized ILTG-NLC and ILTG-NE are shown in Fig. 6. The pattern of the solid lipid showed 4.6°, 5.2°, 6.9°, 8.6°, 10.6°, 11.5°, 12.5°, 13°, 14.2°, 15.2°, 15.7°, 17.1°, 18.6°, 19.4°, 19.9°, 20.4°, 21.1°, 21.9°, and 22.5°. The pattern of the pure-ILTG showed 6°, 7.1°, 7.9°, 8.3°, 11.75°, 12.1°, 12.8°, 14°, 15.6°, 16.5°, 18°, 18.7°, 19.5°, 19.8°, 21.1°, 24.5°, 25.7°, 26.1°, 26.5°, 27°, and 28.2° [36]. The pattern for the drug-lipid physical mixture showed 4.6°, 5.2°, 6.9°, 10.6°, 11.5°, 11.75°, 12.5°, 13.0°, 14°, 15.2°, 17.1°, 18°, 19.5°, 19.8°, 21.1°, 21.7°, 22.3°, 24.5°, 25.7°, 26.1°, and 27°. Overall, the characteristic peak of each of the solid lipids and the ILTG was observed. Through this analysis, we confirmed that the two materials were mixed. In contrast, no sharp characteristic peak for ILTG crystalline was observed in the ILTG-NLC and ILTG-NE. This indicates that ILTG was in a molecular state and not in the crystalline form in the NLCs and NE [37]. The diffraction peak intensity depended on decreasing the solid lipid. The inclusion of ceramide decreased the intensity of the peak. Therefore, the intensity results showed that the crystallinity can be expected to decrease the crystallinity [38]. These results showed a tendency that corroborates the previous DSC data.

1-6. *In Vitro* Skin Permeation

The *in vitro* skin permeation study was performed to investigate the effect of ILTG-loaded formulations. This evaluation was carried out using a Franz diffusion cell (Fig. 7). We prepared a control group using propylene glycol to dissolve ILTG (ILTG-PG). Propylene glycol is widely used as a solvent for dissolving active components in cosmetics. As shown in Fig. 7(a), after 24 h the cumulative permeation of ILTG-PG, ILTG-NLC1, ILTG-NLC2, ILTG-NLC3, and ILTG-NE was 3.99, 8.48, 9.74, 10.09, and 10.12 μg/cm^2, respectively. ILTG-NLC2, ILTG-NLC3 and ILTG-NE showed comparable results. According to previous studies, increasing the liquid lipid would cause it to accumulate on the surface of particles. Thus, the drug release occurs preferentially on the surface of particles. Compared to the NE, the NLCs showed a sustained release profile [39,40]. Fig. 7(b), shows the amount of drug present in the stratum corneum (tape), the epidermis, and dermis (except for stratum corneum, skin), and the amount of drug in the receptor phase that had penetrated the skin (transdermal) by quantitative analysis. The total skin permeation percentage for ILTG-NLC3, ILTG-NLC2, ILTG-NLC1, ILTG-NE, and ILTG-PG was 20.88%, 19.84%, 17.50%, 15.99%, and 7.28%, respectively. The ILTG-NLC3 permeation was approximately three times higher than that of the ILTG through the skin and that of the ILTG-PG (control). The skin permeation is affected by particle size, skin affinity, and skin occlusive effect. Ceramide and cholesterol are lipid components of the stratum corneum and have a marked skin affinity. Additionally, the skin permeation of ILTG was affected by the small particle size of NLC3 [41,42]. These results indicate that increasing the retention time of ILTG on the skin, can be expected to enhance the anti-
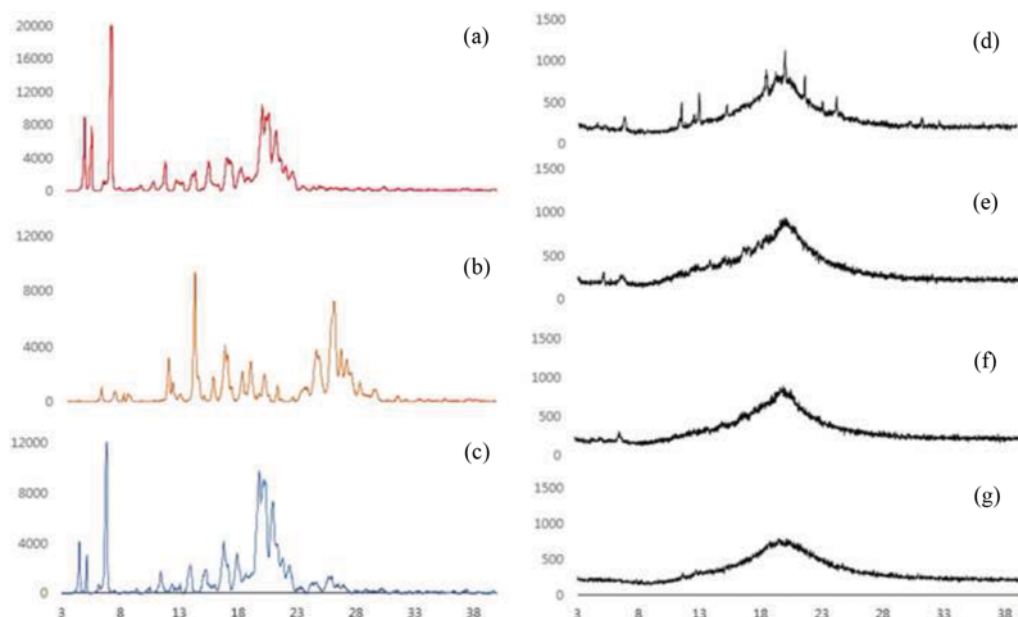

Fig. 6. X-ray diffractograms of (a) solid bulk, (b) isoliquiritigenin (ILTG), (c) physical mixture, (d) ILTG-loaded nanostructured lipid carrier (NLC) 1, (e) ILTG-NLC2, (f) ILTG-NLC3, and (g) ILTG-nanoemulsion (NE).
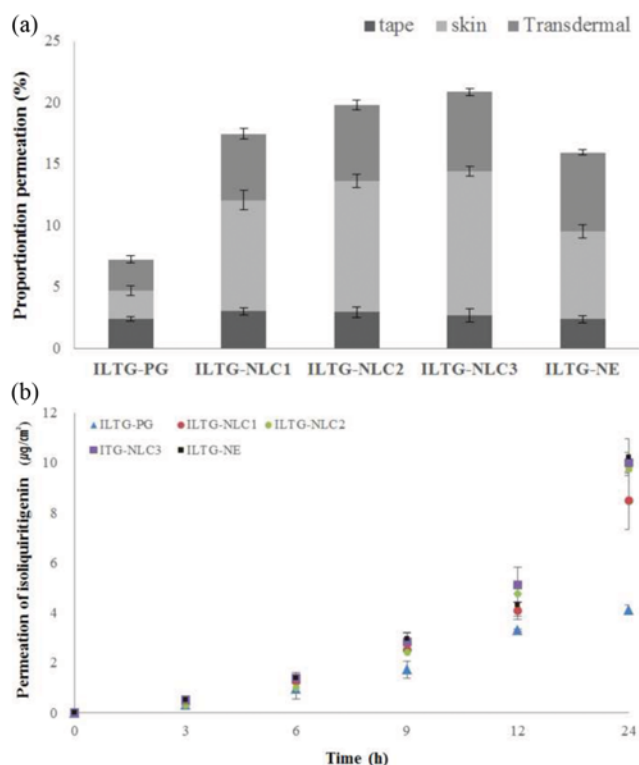
Fig. 7. (a) *In vitro* skin permeation profiles, (b) proportion of permeated isoliquiritigenin (ILTG) from the propylene glycol and various formulations after 24 h (Tape: stratum corneum, Skin: epidermis without stratum corneum and dermis, Transdermal: dissolved in receptor phase through skin).

oxidant and whitening effects of on the skin. We also confirmed that the ceramide-based NLCs are a promising transdermal delivery system and it is possible to control the drug release and permeation, depending on the composition of the lipid ratio.

CONCLUSIONS

Ceramide-based NLCs were developed as a transdermal delivery system for enhancing the permeation of ILTG. We successfully prepared the NLCs by using an ultrasonication method and by blending the solid and liquid lipids in various proportions. In conclusion, we confirmed that the lipid blending ratio was an important factor in determining the physical properties of the NLC formulations. The degree of crystallization affected the drug EE%, release profiles and skin permeation of the formulation. Furthermore, the ILTG-NLCs and ILTG-NE both improved the skin permeation of ILTG. However, the skin permeation of NLC was higher than that of the NE owing to the ceramide content. Based on this normal skin or skin lacking in ceramide could be promising vehicle for the transdermal delivery system of ILTG.

ACKNOWLEDGEMENTS

REFERENCES

1. P. W. Wertz and B. Bergh, *Chem. Phys. Lipids*, **91**, 85 (1988).
2. S. Grayson and P. M. Elias, *J. Invest. Dermatol.*, **78**, 128 (1982).
3. A. D. Nardo, P. Wertz, A. Giannetti and S. Seidenari, *Acta. Derm. Venereol. Suppl. (Stockh)*, **78**, 27 (1998).
4. S. Motta, M. Monti, S. Sesana, L. Mellesi, R. Ghidoni and R. Caputo, *Arch. Dermatol.*, **130**, 452 (1994).
5. K. Perisho, P. W. Wertz, K. C. Madison, M. E. Stewart and D. T. Downing, *J. Invest. Dermatol.*, **90**, 350 (1988).
6. W. Abraham and D. T. Downing, *Pharm. Res.*, **9**, 1415 (1992).
7. S. N. Park, M. H. Lee, S. J. Kim and E. R. Yu, *Biochem. Biophys. Res. Commun.*, **435**, 361 (2013).
8. D. H. Kim, W. R. Park, J. H. Kim, E. C. Cho, E. J. An, J. W. Kim and S. G. Oh, *Colloids Surf., B.*, **94**, 236 (2012).
9. X. Wu and R. H. Guy, *J. Drug. Deliv. Sci. Technol.*, **19**, 371 (2009).
10. Y. R. Neupane, M. Srivastava, N. Ahmad, N. Kumar and A. Bhatnagar, *Int. J. Pharm.*, **477**, 601 (2014).
11. W. S. Choi, H. I. Cho, H. Y. Lee, S. H. Lee and Y. W. Choi, *J. Pharm. Invest.*, **40**, 373 (2010).
12. J. Pardeike, A. Hommoss and R. H. Muller, *Int. J. Pharm.*, **366**, 170 (2009).
13. R. H. Muller, M. Radtke and S. A. Wissing, *Int. J. Pharm.*, **242**, 121 (2002).
14. A. Beloqui, M. A. Solinis, A. Rodriguez-Gascon, A. J. Almeida and V. Preat, *Nanomedicine*, **12**, 143 (2016).
15. X. Zhao, W. Mei, M. Gong, W. Zuo, H. Bai and H. Dai, *Molecules.*, **169**, 775 (2011).
16. X. Zhang, E. D. Yeung, J. Wang, E. E. Panzhinskiy, C. Tong, W. Li and J. Li, *Clin. Exp. Pharmacol. Physiol.*, **37**, 841 (2010).
17. O. Nerya, J. Vaya, R. Musa, S. Izrael, R. Ben-Arie and S. Tamir, *J. Agric. Food Chem.*, **51**, 1201 (2003).
18. S. C. Kim, S. H. Byun, C. H. Yang, C. Y. Kim, J. W. Kim and S. G. Kim, *Toxicology*, **197**, 239 (2004).
19. X. Y. Zhang, H. Qiao, J. M. Ni, Y. B. Shi and Y. Qiang, *Eur. J. Pharm. Sci.*, **49**, 411 (2013).
20. S. J. Kim, S. S. Kwon, S. H. Jeon, E. R. Yu and S. N. Park, *Int. J. Cosmet. Sci.*, **36**, 553 (2014).
21. S. H. Jeon, C. Y. Yoo and S. N. Park, *Colloids Surfaces B: Biointerface.*, **129**, 7 (2015).
22. S. S. Kwon, S. Y. Kim, B. J. Kong, K. J. Kim, G. Y. Noh, N. R. Im, J. W. Lim, J. H. Ha, J. Kim and S. N. Park, *Int. J. Pharm.*, **483**, 26 (2015).
23. S. S. Kwon, B. J. Kong and S. N. Park, *Eur. J. Pharm. Biopharm.*, **92**, 146 (2015).
24. Y. M. Jeong, J. H. Ha and S. N. Park, *J. Ind. Eng. Chem.*, **35**, 54 (2016).
25. V. Teeranachaideekul, P. Boonme, E. B. Souto, R. H. Müller and V. B. Junyaprasert, *J. Control. Release.*, **128**, 134 (2008).
26. K. Jores, W. Mehnert, M. Drechsler, H. Bunjes, C. Johann and K. Mäder, *J. Control. Release.*, **95** 217 (2004).
27. J. Y. Fang, C. L. Fang, C. H. Liu and Y. H. Su, *Eur. J. Pharm. Biopharm.*, **70**, 633 (2008).

28. R. H. Müller, C. Jacobs and O. Kayser, *Adv. Drug Deliv. Rev.*, **47**, 3 (2001).

29. L. R. Rodrigues, *J. Colloid Interface Sci.*, **449**, 304 (2015).

30. N. S. Ranpise, S. S. Korabu and V. N. Ghodake, *Colloids Surf., B: Biointerfaces.*, **116**, 81 (2014).

31. Y. C. Kuo and H. H. Chen, *Int. J. Pharm.*, **365**, 206 (2009).

32. P. K. Gaur, S. Mishra, A. Verma and N. Verma, *J. Exp. Nanosci.*, **11**, 38 (2016).

33. R. Shah, D. Eldridge, E. Palombo and I. Harding, SpringerInternational Publishing (2015).

34. A. Kovacevic, S. Savic, G. Vuleta, R. H. Müller and C. M. Keck, *Int. J. Pharm.*, **406**, 163 (2011).

35. S. B. Han, S. S. Kwon, Y. M. Jeong, E. R. Yu and S. N. Park, *Int. J. Cosmet. Sci.*, **36**, 588 (2014).

36. B. Li, B. Liu, J. Li, H. Xiao, J. Wang and G. Liang, *Int. J. M. Sci.*, **16**, 17999 (2015).

37. Y. R. Neupane, M. Srivastava, N. Ahmad, N. Kumar, A. Bhatnagar and K. Kohli, *Int. J. Pharm.*, **477**, 601 (2014).

38. R. N. Shamma and M. H. Aburahma, *Int. J. Nanomedicine.*, **9**, 5449 (2014).

39. M. Pradhan, D. Singh and M. R. Singh, *Chem. Phys. Lipids*, **186**, 9 (2015).

40. H. Chen, Y. Wang, Y. Zhai, G. Zhai, Z. Wang and J. Liu, *Colloids Surf., A: Physicochem. Eng. Asp.*, **465**, 130 (2015).

41. E. B. Souto, S. A. Wissing, C. M. Barbosa and R. H. Müller, *Int. J. Pharm.*, **278**, 71 (2004).

42. Y. Zhai and G. Zhai, *J. Control. Release.*, **193**, 90 (2014).